Geometrical optimization of helical flow in grooved micromixers†

N. Scott Lynn and David S. Dandy*

Received 18th January 2007, Accepted 20th March 2007
First published as an Advance Article on the web 11th April 2007
DOI: 10.1039/b700811b

Owing to the enhancement of surface effects at the micro-scale, patterned grooves on a micro-channel floor remain a powerful method to induce helical flows within a pressure driven system. Although there have been a number of numerical studies on geometrical effects concerning fluid mixing within the staggered herringbone mixer, all have focused mainly on the groove angle and depth, two factors that contribute greatly to the magnitude of helical flow. Here we present a new geometrical factor that significantly affects the generation of helical flow over patterned grooves. By varying the ratio of the length of the grooves to the neighboring ridges, helical flow can be optimized for a given groove depth and channel aspect ratio, with up to 50% increases in transverse flow possible. A thorough numerical study of over 700 cases details the magnitude of helical flow over unsymmetrical patterned grooves in a slanted groove micro-mixer, where the optimized parameters for the slanted groove mixer can be translated to the staggered herringbone mixer. The optimized groove geometries are shown to have a large dependence on the channel aspect ratio, the groove depth ratio, and the ridge length.

1. Introduction

It is recognized that mixing plays an important role in the growing use of microfluidic devices for lab-on-a-chip applications.[1,2] For applications ranging from DNA separation and amplification to protein crystallization and kinetics studies, the performance of a lab-on-a-chip device is directly related to the rate at which two or more fluids can be mixed. Because of the small dimensions of micro-channels as well as the limited range of obtainable linear flow rates, flow in micro-channels is confined to the laminar regime and mixing is dominated by molecular diffusion. Microfluidic mixing may be accomplished using a variety of approaches. Active mixers may rely on external energy sources, such as electro-osmotic flow,[3–5] external pressure gradients,[6,7] and electrokinetic instabilities[8,9] to perturb fluid streamlines into a mixing state. Unlike their active counterparts, passive mixers utilize existing geometries within a micro-channel to mix externally pumped fluids. Efficient passive mixing in planar micro-channels may be accomplished *via* flow-through spiral-type micro-channels,[10,11] as well as *via* gas–liquid[12] or liquid–liquid[13] multi-phase flow. More complicated three-dimensional micro-channel systems have also been used to mix fluids *via* chaotic advection[14] and other split and recombine methods.[15,16]

Perhaps the best known examples pertaining to passive microfluidic mixing are the staggered herringbone mixer (SHM)[17] and the slanted groove micro-mixer (SGM).[18] The SGM consists of diagonal grooves embedded into the floor of a micro-channel situated at an angle θ with respect to the axial direction, whereas the SHM grooves exist in a herringbone pattern. The oblique grooves serve to transport fluid from the apex of the groove structure to the downstream edges of the micro-channel. As a result, fluid near the top of the channels will re-circulate in the opposite direction, and an overall helical flow pattern is created. The herringbone pattern on the SHM serves to generate two counter-rotating helical flows, such that a chaotic flow profile may be created by alternating the asymmetry of the herringbones along the length of the micro-channel. Owing to its simple planar design, the SHM is readily fabricated using standard soft lithographic methods,[19] thus making a convenient choice for lab-on-a-chip applications requiring rapid mixing of two or more liquids, such as the lysis of whole blood using de-ionized water.[20] Several passive mixer designs have evolved from the original SGM design: Kim *et al.* placed alternating barriers above the slanted grooves to achieve enhanced mixing effects with the barrier embedded mixer (BEM),[21] and Sato *et al.* fabricated PDMS micro-channels with slanted grooves on the sidewalls as well as the channel floor to achieve increases in bulk helical flow.[22,23]

To date, there have been a number of theoretical, experimental, and numerical studies aimed at the optimization of SHM- and SGM-type devices. Stroock *et al.* developed an analytical solution to the Stokes equations to quantify non-axial flow over sinusoidal modulated surfaces,[18] and later showed that flow over oblique grooves may be accurately modeled using a superposition of the analytical 2-D lid-driven cavity solution with the Fourier series solution to Poiseuille flow in rectangular ducts.[24] Owing to the low Reynolds number flows and simple geometries, the SHM and SGM are perfect candidates for study with computational fluid dynamics (CFD), usually *via* finite element, finite volume, or lattice Boltzmann methods. Several CFD studies on the SHM report consistent mixing profiles between computational and experimental methods *via* the solution of the convection–diffusion

Department of Chemical & Biological Engineering, Colorado State University, CO 80523, USA

† Electronic supplementary information (ESI) available: typical computational domain of SGM, graph of η *vs.* groove number, graph of η *vs.* (h/w) and comparison of helical flow characterization methods. See DOI: 10.1039/b700811b

equation for the concentration field.[25,26] Although these methods are particularly useful for visualization of the flow field, numerical diffusion errors are typically high and quantification of the mixing efficiency is difficult. To avoid these numerical errors, several studies have utilized particle tracking methods to characterize the mixing properties of the SHM and SGM in more detail. Kang *et al.*[27] utilized colored particle tracers to display excellent resolution of the multi-cycle SHM mixing profile, Camesasca *et al.*[28] utilized statistical entropy of particle tracers to evaluate the mixing efficiency of the original SHM design, and Aubin *et al.*[29] displayed Poincaré maps for the original SHM and SGM designs in addition to an analysis of the magnitude of the rate of deformation tensor along the length of the mixer.

In addition to validation of the flow field, recent work has been focused on the optimization of SGM and SHM devices. Both Wang *et al.*[30] and Hassell *et al.*.[31] studied the effects of the groove depth to channel height ratio in SGM designs. Li *et al.*[32] used a lattice Boltzmann method to study effects of the width fraction of the long arm and the number of grooves per half-cycle on SHM designs. Additionally, Aubin *et al.*[33] used particle tracking methods to study the effects of the groove spacing on the same SHM designs. In the most complete optimization study to date, Yang *et al.*[34] used the Taguchi method to study the effects of the groove depth ratio, the width fraction of the long arm, the channel height to width aspect ratio, and the groove intersection angle on helical flow within the SHM. These published studies agree on several conclusions: (1) the mixing properties of the SHM are much more efficient than those of the SGM, (2) the mixing properties of the SHM are optimized when the width fraction of the long arm is approximately 2/3, (3) non-axial flow is maximized over a groove intersection angle of 45°, (4) the magnitude of helical flow is weakly dependent on the channel aspect ratio, and (5) the magnitude of helical flow is strongly dependent (asymptotically) on the groove depth ratio. It is consistently observed that as helical flow increases (or the magnitude of flow within the grooves), the rate of mixing within the SHM increases, and the overall SHM length needed for complete mixing decreases. Although a number of different numerical studies exist concerning the SHM, little is known regarding the effect of the groove spacing on helical flow, and there are no comprehensive design parameters associated with the overall SHM geometries.

To date, all published experimental and numerical studies concerning flow over patterned grooves have involved symmetric grooves, for which the groove and ridge lengths are equal. In this study, computational fluid dynamics is applied to demonstrate that the magnitude of helical flow is strongly dependent on the groove spacing within a SGM, and that the equal spacing used in all previous studies does not provide an optimum design. Further, the optimum groove spacing is strongly dependent on both the channel aspect ratio and the groove depth to channel height ratio. A full numerical study details the magnitude of helical flow over uneven patterned grooves in the SGM, where the optimized parameters can be used to optimize flow within the SHM. Helical flows over 700 different SGM geometries were computed within this study.

2. Motivation

Previous computational studies on flow within the SHM have shown particle pathline plots in which there is a small scale helical motion situated directly over the patterned grooves.[30,32,34] In these studies, no characterization of this flow mode was carried out. An example of this flow pattern is shown in Fig. 1, illustrating pathline plots within a SGM (computed in this study with methods discussed below), and can be described as follows: fluid flow directly over the grooves is viscously affected by flow within the grooves directed toward the channel walls, whereas flow between the grooves (over the ridges) is viscously affected by the recirculation pattern above, flowing in the opposite direction. The fluid directly over the ridges appears to inhibit the overall non-axial transport of fluid in the direction of the grooves, thus limiting the total magnitude of helical flow within the device. Because the overall goal is to maximize the non-axial convective transport of fluid within the grooves, it is reasonable that the ridge length should be minimized to acceptable lengths that can be readily fabricated.

Fig. 2 displays the geometries considered in this study. Rather than utilize notations described in previous studies, a

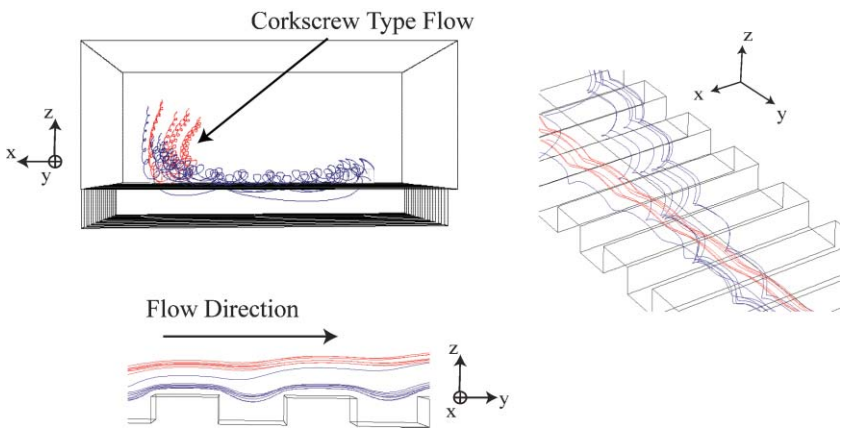

Fig. 1 Pathlines of fluid flow over patterned grooves. Flow just over the grooves is shown in blue, and the resulting re-circulation flow is shown in red.

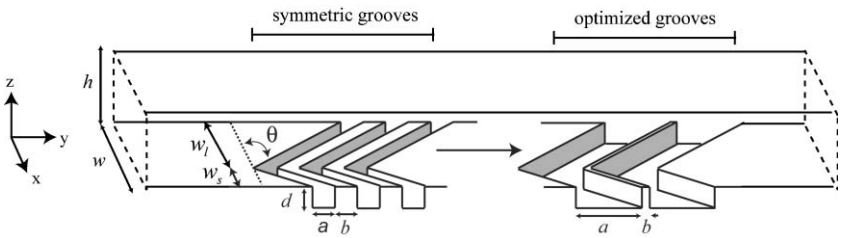

Fig. 2 The geometric parameters used within this study.

new set of geometries has been adopted that are directly related to the fabrication of SHM type devices, namely the spin coat thickness and photo-mask design. Previous studies have shown that helical flow is maximized when the groove intersection angle $\theta = 45^\circ$, therefore that value has been used in this study. Along with the channel height (h) and width (w), additional geometric parameters are the groove depth (d), the groove width (a), and the ridge width (b). Mixers are classified here according to their groove depth to channel height ratio (d/h), the channel aspect ratio (h/w), and the groove and ridge to width ratios (a/w, b/w). Because the limits of $b/a \rightarrow 0$ and $b/a \gg 1$ will produce Poiseuille flow profiles containing no helical flow, there must exist an optimum ratio b/a that maximizes helical flow over the grooves for a specific value of b. Thus, this study involves finding the optimized groove spacing (a/w) for a given SHM type device, and how that groove spacing relates to channels with specific d/h, h/w, and b/w ratios.

3. Numerical methodology

Because of its geometrical simplicity, the slanted groove mixer is utilized for the study of geometrical effects on the magnitude of helical flow. The magnitude of helical flow within the SGM is closely related to that within the SHM, where optimized geometries for the SHM can be derived from those optimized from the SGM (to be further discussed later). The finite volume CFD package FLUENT was used to simulate the 3-D velocity field through a planar SGM device consisting of one inlet and one outlet. The entry and exit lengths of the channel were constant at $w/2$, and the length of the channel containing grooves was a minimum of $7w$, the minimum lengths to produce a fully developed flow profile. The CFD preprocessing package Gambit® was used to discretize the SGM into 6-node trihedral elements with typical cell dimensions of $w/50$. For geometries with small features (small b/w, a/w, d/h values), a minimum of 8 elements were placed along the groove and ridge walls (x and z-directions), which has been determined in this system to be sufficient resolution to ensure the predicted flow field is independent of the mesh density. This mesh density corresponds to a minimum of 1.5 million elements per computational simulation. The boundary conditions for the channel inlet were v_y = constant, $v_x = v_z = 0$, where it was determined that the constant velocity inlet condition had no impact on the magnitude of helical flow downstream. A constant pressure condition on the outlet was used along with a no-slip condition on all surfaces, with water at 25 °C and 1 atm used for the operating fluid. The SIMPLEC method was used for pressure–velocity coupling, with a second-order upwind discretization scheme for the velocity calculations. The simulations were considered converged when the normalized residuals for the velocities and continuity fell below 10^{-7} and 10^{-4}, respectively.

For purposes of consistency, the magnitude of non-axial flow within the SGM has been analyzed by calculating the magnitude of re-circulating flow towards the center of the channel. Fig. S1 in the ESI† displays a computational domain of a typical SGM in this study, together with the non-axial (x) velocity contour profile in the center of the channel. The x-velocity profile along the midplane of the SGM is divided into planes correlating to one groove and its neighboring ridge. For each individual plane the non-axial volumetric flow (Q_n) is

$$Q_n = \int_y \int_z [v_x(x,y,z)]_{v_x<0} \mathrm{d}y\mathrm{d}z, \tag{1}$$

where restricting the integration to values of $v_x < 0$ ensures the quantification of fluid passing through the midplane in one direction only. To quantify the magnitude of helical flow within the SGM, the ratio of non-axial (Q_n) to axial flow (Q_a) is calculated as

$$\eta = \frac{Q_n w}{Q_a(a+b)} = \frac{Q_n}{\langle v_y \rangle h(a+b)}, \tag{2}$$

where Q_n and Q_a have been normalized by the groove-ridge length ($a + b$) and channel width w, respectively. The ratio η provides a reliable measure of the relative magnitude of secondary re-circulation flow, and thus the total magnitude of helical flow, above the grooves. Also, η is independent of the volumetric flow rate through the SGM (for $Re < 100$, where $Re = \langle v_y \rangle w/\nu$ for a fluid with kinematic viscosity ν), highlighting the insensitivity of the flow profile to the Reynolds number within SHM-type devices. For all cases considered in this study, $Re = 0.02$. Fig. S2 in the ESI† displays η as a function of groove number for several typical SGM geometries in this study; η reaches a maximum value within w axial lengths from the start and end of the groove cycle, where the variation between the maximum value and that in the center of the groove cycle varies by less than 5%. The drop off in the magnitude of η as the groove cycle ends is due to the dissipation of the effects of the flow rate through the grooves, as non-axial flow in the opposite direction is spread out along the axial length of the channel. This observation is consistent with the work by Yang *et al.*,[34] in which the volumetric flow rate through the first and last grooves per half-cycle were higher than the center grooves. The values of η reported in this

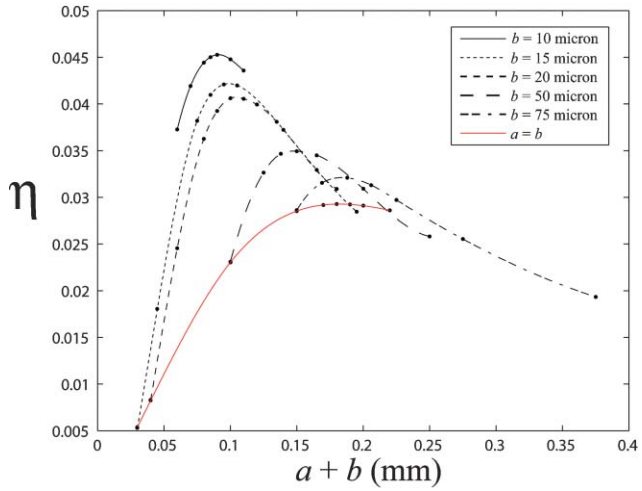

Fig. 3 η *vs.* the total groove length ($a + b$) for several SGMs with h = 80 μm, w = 200 μm, and d = 20 μm. The red line indicates the constrained SGM, with $a = b$.

study are the maximum values of η *vs.* groove number (as shown in Fig. S2†).

Previous characterization of helical flow over patterned grooves included the maximum shear rate $(v_x/v_y)_{max}$, located near the top of the channel.[18,25] This characterization can lead to erroneous results, as two SGMs with different geometries can produce the same maximum value of $(v_x/v_y)_{max}$, yet have very different mixing properties. In general, geometrical changes in the SGM produce similar trends in both $(v_x/v_y)_{max}$ and η: however, characterization *via* η gives a more accurate representation of helical flow within a SHM. (Additional details on these characterization methods may be found within the ESI.) Eqn 1 is similar to the methods of helical flow characterization employed by Yang *et al.*[34] in their analysis of the volumetric groove flow rate for different mixer geometries. Actually, this approach accounts for the *effects* of the flow within the grooves, furthermore accounting for changes in the groove geometries, to provide a common, platform-independent metric for the comparison of different mixers. The relationship between helical flow rates and mixing efficiency within SHM type devices have been previously reported.[24,33,34] Thus, larger values of η translate to higher rates of mixing in a SHM within the individual cycles, which correlate to a smaller length of a SHM needed for complete mixing.

4. Helical flow within a SGM

For a SGM with specific d/h and h/w ratios, there will exist an optimum groove spacing that maximizes helical flow. To determine this optimum spacing, helical flow within several SGMs with varying groove geometries (constant d/h and h/w ratios) is calculated. Fig. 3 displays η *vs.* ($a + b$) for several values of a set ridge length b (including the case $a = b$) for a SGM with dimensions h = 80 μm, w = 200 μm, and d = 21 μm. The channel aspect ratio h/w = 0.4 and groove depth ratio d/h = 0.2625 correspond well to previous experimental and numerical studies.[18,25] It is observed that, as b decreases, the maximum obtainable value of η increases by up to 50% of the base ($a = b$) case. For example, the SGM base case yields a maximum ratio η = 0.03 at a groove spacing of $a = b$ = 78 μm, whereas the optimized SGM (b = 10 μm) exhibits a maximum ratio η = 0.045 at a groove spacing of a = 88 μm. It can be seen that as b is minimized, the maximum obtainable value of η increases, and the total groove spacing ($a + b$) at which this maximum value occurs decreases, allowing for an increase in grooves per cycle length. To further highlight this effect of optimizing the groove spacing, Fig. 4 displays normalized concentration distributions along two SGMs, one of which has been optimized for helical flow. The CFD simulation pertains to a generic solute (diffusion coefficient $D = 10^{-10}$ m^2 s^{-1}, Pe_{mesh} = 4) initially segregated on one side of the SGM inlet ($\langle v_y \rangle$ = 1 mm s^{-1}), where the SGM has dimensions h = 60 μm, w = 200 μm, and d = 30 μm. Flow through the optimized SGM undergoes an approximately 360° twist (η = 0.09) within 2 mm of axial length, whereas flow through a SGM with symmetric

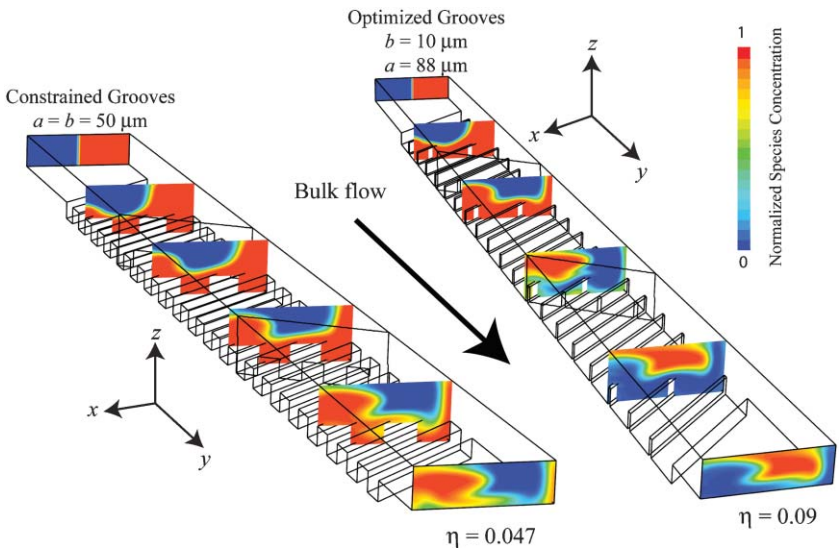

Fig. 4 Comparison of concentration distributions displaying helical flow between a SGM with constrained grooves (left) and optimized grooves (right). The SGM has absolute dimensions of w = 200 μm, h = 60 μm, and d = 30 μm.

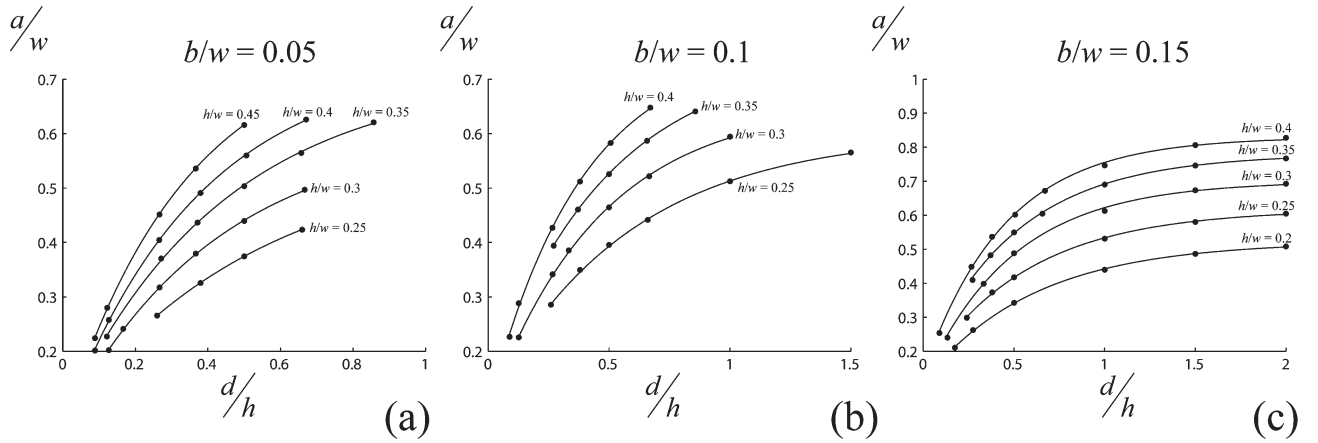

Fig. 5 Optimized groove geometries, shown as *a*/*w vs. d*/*h*, for several different channels of varying *h*/*w* and *b*/*w*.

grooves ($a = b$) undergoes only a 180° twist ($\eta = 0.047$) for the same axial channel length. Fig. 4 displays the relationship between η and the total magnitude of helical flow within a SGM, where it appears that η is proportional to the fluid twist per axial length of channel; however, this relationship has yet to be further clarified.

It is now clear that an increase in helical flow within a SGM can be accomplished in a straightforward manner by optimizing the geometrical parameters of the grooves present on the micro-channel floor. These optimized grooves lead to an increase in the re-circulatory flow above the grooves, as well as flow within the grooves themselves. Fig. 3 highlights the optimized parameters for a channel with geometric ratios $h/w = 0.4$ and $d/h = 0.2625$. Optimized groove geometries of micro-channels with varying *h*/*w* and *d*/*h*, along with the resulting effects on η, will be discussed further in the next section.

5. Geometric optimization

It remains important to maintain flexibility in SHM or SGM geometries during the design of lab-on-a-chip processes, and to this end a wide range of geometric ratios were chosen for this study. The range of channel aspect ratios for this study was chosen as $0.2 < h/w < 0.45$. For each *h*/*w* value, a range of groove depth ratios was chosen as $0.09 < d/h < 2$, at which three *b*/*w* values were studied: $b/w = 0.05$, 0.10, and 0.15. Some of the parameter space was not studied due to the potential fabrication difficulties associated with high aspect ratio grooves (channels with low *b*/*w* and high *d*/*h* ratios). A minimum of 6 CFD cases corresponding to geometries with varying *a*/*w* were computed for each micro-channel geometry (*h*/*w*, *d*/*h*, *b*/*w*). For these cases, a cubic spline function was fit to η as a function of *a* to evaluate the optimized *a*/*w* value for that geometry. For randomly selected channel geometries, the difference between the optimized *a*/*w* value computed from 6 CFD cases and the value utilizing 10 or more cases was less than 4%.

Optimization of groove geometry with depth ratio *d*/*h*

The groove depth ratio has previously been found to be the most sensitive parameter affecting the magnitude of helical flow over grooved surfaces.[30,31,33,34] To date there has been no study on the dependency of the groove geometries on the *d*/*h* ratio. Fig. 5 displays the optimized groove geometries, shown as *a*/*w vs. d*/*h*, for a wide range of *h*/*w* and *b*/*w* values. As expected, *a*/*w* increases asymptotically with increasing *d*/*h*, due to the fact fluid near the bottom of deeper grooves has less impact on the flow profile through the SGM. The groove length is also dependent on the ridge length used, as for constant *h*/*w* and *d*/*h* values, *a*/*w* increases with increasing values of *b*/*w*. For precise fabrication of optimized mixing devices between the data points shown in figure 5, the optimized groove geometries may be fit to the asymptotic relationship:

$$\frac{a}{w} = a_0\left[1 - \exp\left(-a_1\left(\frac{d}{h}\right)^{a_2}\right)\right] \quad (3)$$

Non-linear regression was used to calculate the parameters a_0, a_1, and a_2, and these values are shown in Table 1. All of the curves (constant *h*/*w*, *b*/*w*) resulting from eqn 3 yielded non-linear regression R^2 coefficient values greater than 0.992. The asymptotic value a_0 is found to be proportional to *h*/*w*, as seen in Fig. 5(c); however, this relationship has yet to be confirmed for values outside the range considered in this study. Eqn 3 is not meant to elucidate the physical relationships between the parameters important to helical flow within a SGM, it is simply a sizing guide for optimized fabrication of these devices.

Table 1 Non-linear regression parameters, 95% confidence intervals shown in parentheses

h/*w*	*b*/*w*	a_0	a_1	a_2
0.25	0.05	0.661 (0.19)	1.39 (0.77)	0.741 (0.14)
0.30	0.05	0.70 (0.030)	1.70 (0.13)	0.777 (0.019)
0.35	0.05	0.793 (0.010)	1.72 (0.049)	0.772 (0.008)
0.4	0.05	0.824 (0.023)	1.96 (0.128)	0.802 (0.016)
0.45	0.05	0.878 (0.047)	2.13 (0.25	0.816 (0.030)
0.25	0.1	0.637 (0.020)	1.62 (0.138)	0.743 (0.039)
0.30	0.1	0.733 (0.027)	1.67 (0.147)	0.734 (0.027)
0.35	0.1	0.814 (0.030)	1.74 (0.160)	0.74 (0.032)
0.4	0.1	0.915 (2.0e-6)	1.64 (4.9e-6)	0.718 (2.9e-6)
0.2	0.15	0.555 (0.019)	1.56 (0.150)	0.686 (0.041)
0.25	0.15	0.641 (0.010)	1.75 (0.096)	0.723 (0.029)
0.3	0.15	0.724 (0.019)	1.87 (0.18)	0.772 (0.050)
0.35	0.15	0.793 (0.011)	2.03 (0.120)	0.787 (0.038)
0.4	0.15	0.865 (0.021)	1.97 (0.160)	0.726 (0.040)

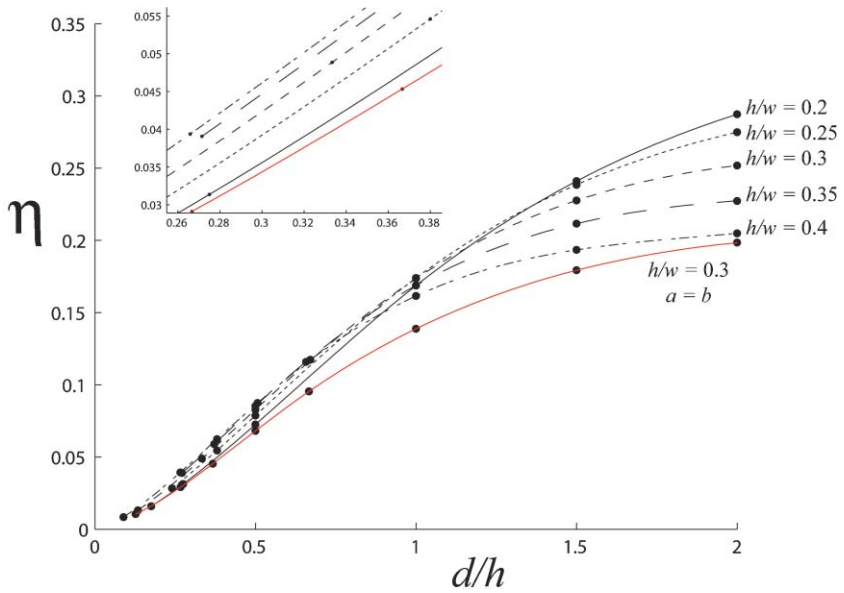

Fig. 6 η *vs.* d/h shown for a SGM with $b/w = 0.15$, with optimized groove geometries corresponding to the points in figure 8(c). The red line relates to a constrained SGM with ($a = b$). The inset displays R *vs.* d/h for values of $0.26 < d/h < 0.04$.

Fig. 6 shows η as a function of d/h for the optimized a/w values shown in Fig. 5(c); η increases linearly at low groove depth ratios ($d/h < 0.6$), followed by an asymptotic increase at higher d/h ratios. This result parallels that of Stroock *et al.*[18] along with previous numerical studies,[25,30,31] likely because η follows the same trends as the maximum shear rate (v_x/v_y) concerning flow over patterned grooves. As with the asymptotic relationship seen in Fig. 5, as d/h increases there is a limit to the obtainable volumetric flow within the grooves, and thus a limit to what values η can attain. Due to the mechanical stability of the ridges themselves, the asymptotic maximum helical flow strength with respect to the groove depth ratio is most likely out of the range of devices readily fabricated *via* soft lithographic methods; however, these structures very well may be obtainable utilizing other micro-channel substrates. Interestingly, for low aspect ratio channels, the asymptotic maximum for the groove length occurs at d/h values much lower than the maximum for helical flow. Thus, there is a limit for which the groove spacing becomes constant, yet η still increases with increasing d/h. Fig. 6 highlights the effect of optimizing the groove spacing, and as for channels with $h/w = 0.3$, a SGM with constant ridge ratio $b/w = 0.15$ displays helical flow magnitudes approximately 25% higher than a channel with symmetric ridges (red line). This increase in η for optimized groove spacing becomes greater as b/w is further minimized.

Optimization of channel aspect ratio *h/w* with groove depth ratio *d/h*

The sensitivity of helical flow on the channel aspect ratio can be seen in Fig. 6. At low groove depth ratio values ($d/h < 0.5$), higher aspect ratio channels exhibit the highest rates of helical flow. As the groove depth ratio is increased, an inversion occurs and helical flow becomes greater in lower aspect ratio channels. Thus, for a specific groove depth ratio, there exists an optimum channel aspect ratio for maximizing helical flow. Fig. S3 in the ESI† shows helical flow strength as a function of the channel aspect ratio for several groove depth ratio values ($b/w = 0.15$). As the groove depth ratio is increased, the optimum channel aspect ratio decreases, where at groove depth ratios of $d/h > 1.6$ and $d/h < 0.6$, the maximum lies outside of the range considered in this study. Despite the lack of data for low values of d/h, it is apparent that the channel aspect ratio has a strong affect on helical flow. For example, for channels with $d/h = 0.4$ there is a 25% increase in helical flow from an aspect ratio $h/w = 0.2$ ($\eta = 0.053$) to an aspect ratio of $h/w = 0.4$ ($\eta = 0.066$). The optimized parameters shown in Fig. S3† are displayed in Table 2. For the range of parameters used in this study, the optimized h/w values are independent of b/w. A previous study, in which only three channel aspect ratios were examined, determined that this parameter had minimal impact on helical flow.[34] The data in

Table 2 η *vs.* h/w optimization parameters

d/h	opt. h/w	η_{max}
0.3	>0.4	n.a.
0.4	>0.4	n.a.
0.5	0.393	0.086
0.6	0.367	0.105
0.7	0.348	0.124
0.8	0.320	0.141
0.9	0.289	0.158
1.0	0.271	0.174
1.1	0.255	0.190
1.2	0.234	0.204
1.3	0.232	0.217
1.4	0.222	0.230
1.5	0.212	0.241
1.6	0.206	0.252
1.7	<0.2	n.a.
1.8	<0.2	n.a.
1.9	<0.2	n.a.
2.0	<0.2	n.a.

Table 2 demonstrate that this conclusion is not correct. Not only does h/w have a strong impact on helical flow over patterned grooves, but the optimized h/w value is also dependent on d/h. Current work is focused on elucidating the limits of the optimized aspect ratio when $d/h \rightarrow 0$ or $d/h \gg 1$.

The results shown in Fig. 5, Fig. 6, and Table 2 display the effects of d/h, h/w, b/w, and a/w on the total helical flow magnitude η within a SGM. Of the four dimensionless parameters, helical flow is most sensitive to d/h; however helical flow can be significantly increased by minimizing b/w while simultaneously optimizing h/w and a/w. When designing devices that utilize patterned grooves for lateral transport of fluid, all of the above geometric parameters need to be taken into account for complete optimization of the device.

Implications for the staggered herringbone mixer

The optimization procedure described in this study was specific to the SGM; however, these techniques can be applied to any device using patterned grooves for non-axial fluid transport purposes (specifically the BEM and SHM). Optimizing fluid in the BEM is straightforward, and the SHM can be thought of as two SGM devices adjacent to one another with aspect ratios h/w_s and h/w_l (Fig. 2), where the asymmetry of the herringbone pattern is such that $w_l = p\ w$. For these two sections, $h/w_s = 2h/w_l$, and helical flow over the long arm will most likely be different from that over the short arm (*cf.* Fig. S3†), in contradiction with the boundary conditions used in the analytical model developed by Stroock *et al.*[24] It is reasonable to expect that fluid flow within the long arm of the SGM is the primary mechanism for fluid mixing, thus the SHM should be sized *via* h/w_l, b/w_l, and a/w_l for flow optimization over the long arm, where the short arm retains the same groove geometries a, b, and d. Computational studies of helical flow on the long arm of the SHM varied by less than 3% of that within the SGM when $(a/w_l)_{SHM} = (a/w)_{SGM}$, $(h/w_l)_{SHM} = (h/w)_{SGM}$, and $(b/w_l)_{SHM} = (b/w)_{SGM}$ within SHM and SGM devices with the same d/h value (data not shown). For SHM type devices with grooves placed on more than one wall, such as those displayed by Sato *et al.*,[22,23] we expect the optimization procedure to be equivalent to that shown above, where the defining ratios of such a mixer would remain d/h, h/w, and b/w.

Since the magnitude of helical flow within a SHM device is certainly important, other design properties also contribute significantly to the creation of chaotic flow. One important factor is the number of grooves per half-cycle (N). Several groups have studied the effect of N on the mixing performance of SHM-type devices.[32,33] Li *et al.* found that the mixing performance was dependent on N, as long as N was above a particular value (in their case, $N \geqslant 4$). The values of N that Aubin *et al.* used were much higher (N = 10, 20, and 30), and no dependence of the mixing performance on N was found. These results suggest that there exists not a critical value of N, but a critical length of each half-cycle (L_c), below which the mixing performance of the SHM will suffer. By optimizing the geometries of the SHM using the relationships found in Fig. 5 and Table 2, the rate at which fluid is transferred laterally across the floor, as well as the exchange of fluid between the two counter-rotating currents, will be maximized. This should serve to have a profound effect on the mixing performance of such devices, since the value of L_c for an optimized SHM should be well below that of previous SHM designs. Current studies indicate that the values of L_c in optimized SHM devices may be as small as $L_c = w$, long enough to necessitate only several grooves per half-cycle. This hypothesis has not been tested, and is the focus of future work.

6. Conclusion

Helical flow is investigated within the slanted groove mixer (SGM), whose geometry can be completely described by the ratios d/h, h/w, a/w, and b/w. The relative helical flow magnitude is described by the parameter η, which is the ratio of transverse to axial flow rate over individual grooves, normalized by the length of the groove and neighboring ridge as well as the width of the micro-channel. Over 700 channels with differing geometries (as described by d/h, h/w, a/w, and b/w) were studied *via* computational fluid dynamics (CFD) using the commercial package FLUENT.

Helical flow within a SGM is found to be dependent on all four geometric ratios. For a SGM with specific values of d/h, b/w, and h/w, there exists an optimum groove geometry a/w that will maximize helical flow. By removing the constraint that grooves and ridges remain symmetric (*i.e.*, the base case $a = b$), as has been used in all previous studies, non-axial fluid transport can be substantially increased. In particular, helical flow increases significantly as the ridge length ratio b/w is minimized, where the optimum value of a/w is further dependent on the specific ratios d/h and h/w. Fig. 5 and S3†, (or Tables 1 and 2) can be directly applied as design criteria for a SGM. After the values for the groove depth (d) and channel height (h) are chosen (the two geometries defined by the Su-8 spin coating process, for example), the channel width can be optimized *via* Table 2, and the groove geometries can be interpolated using Table 1. Although the groove geometries will be dependent on specific lithographic capabilities, larger values of b/w can still provide a significant increase from symmetric grooves, providing the grooves are sized appropriately. For other fabrication methods, such as micro-milling, fabrication of small a/w ratios can be a challenge, as the smallest available cutting tool is approximately 100 μm. Thus, micro-milling fabrication of optimized mixers whose overall size is relatively small might not be possible (for example, $w < 200$ μm).

While this study deals specifically with the optimization of helical flow within a slanted groove mixer, the data in Fig. 5 and S3†, or Tables 1 and 2, can also be used to optimize flow within a staggered herringbone mixer (SHM). Rather than normalizing geometric parameters with the total width w of the channel, the SHM is sized to the width of the long arm w_l. Thus a/w_l, h/w_l, and b/w_l are sized according to Fig. 5 and S3†. By optimizing the long arm of the SHM, the critical length for each half-cycle of grooves is expected to decrease: however, this has yet to be confirmed. Regardless, optimized flow within a SHM correlates to a higher magnitude of non-axial flow located within the grooves, which has been shown in the past to provide faster mixing rates. This study presents the first

sizing guide for optimization of flow over patterned grooves, such that the optimization procedure will provide faster rates of non-axial transport—and hence, mixing—within the SGM, SHM and BEM.

Acknowledgements

This work was supported by NIH grant number EB00726.

References

1 H. A. Stone, A. D. Stroock and A. Ajdari, *Annu. Rev. Fluid Mech.*, 2004, **36**, 381–411.
2 J. M. Ottino and S. Wiggins, *Philos. Trans. R. Soc. London, Ser. A*, 2004, **362**, 923–935.
3 T. J. Johnson, D. Ross and L. E. Locascio, *Anal. Chem.*, 2002, **74**, 45–51.
4 H. Y. Wu and C. H. Liu, *Sens. Actuators, A*, 2005, **118**, 107–115.
5 J. L. Lin, K. H. Lee and G. B. Lee, *Electrophoresis*, 2005, **26**, 4605–4615.
6 A. Dodge, M. C. Jullien, Y. K. Lee, X. Niu, F. Okkels and P. Tabeling, *C. R. Phys.*, 2004, **5**, 557–563.
7 X. Z. Niu and Y. K. Lee, *J. Micromech. Microeng.*, 2003, **13**, 454–462.
8 M. H. Oddy, J. G. Santiago and J. C. Mikkelsen, *Anal. Chem.*, 2001, **73**, 5822–5832.
9 N. Sundaram and D. K. Tafti, *Anal. Chem.*, 2004, **76**, 3785–3793.
10 F. Jiang, K. S. Drese, S. Hardt, M. Kupper and F. Schonfeld, *AIChE J.*, 2004, **50**, 2297–2305.
11 A. P. Sudarsan and V. M. Ugaz, *Lab Chip*, 2006, **6**, 74–82.
12 A. Gunther, S. A. Khan, M. Thalmann, F. Trachsel and K. F. Jensen, *Lab Chip*, 2004, **4**, 278–286.
13 H. Song, J. D. Tice and R. F. Ismagilov, *Angew. Chem., Int. Ed. Engl.*, 2003, **42**, 768–772.
14 R. H. Liu, M. A. Stremler, K. V. Sharp, M. G. Olsen, J. G. Santiago, R. J. Adrian, H. Aref and D. J. Beebe, *J. Microelectromechan. Syst.*, 2000, **9**, 190–197.
15 H. Chen and J. C. Meiners, *Biophys. J.*, 2004, **86**, 482A–482A.
16 D. Therriault, S. R. White and J. A. Lewis, *Nat. Mater.*, 2003, **2**, 347–347.
17 A. D. Stroock, S. K. W. Dertinger, A. Ajdari, I. Mezic, H. A. Stone and G. M. Whitesides, *Science*, 2002, **295**, 647–651.
18 A. D. Stroock, S. K. Dertinger, G. M. Whitesides and A. Ajdari, *Anal. Chem.*, 2002, **74**, 5306–5312.
19 Y. N. Xia and G. M. Whitesides, *Annu. Rev. Mater. Sci.*, 1998, **28**, 153–184.
20 P. Sethu, L. L. Moldawer, M. N. Mindrinos, P. O. Scumpia, C. L. Tannahill, J. Wilhelmy, P. A. Efron, B. H. Brownstein, R. G. Tompkins and M. Toner, *Anal. Chem.*, 2006, **78**, 5453–5461.
21 D. S. Kim, S. W. Lee, T. H. Kwon and S. S. Lee, *J. Micromech. Microeng.*, 2004, **14**, 798–805.
22 H. Sato, S. Ito, K. Tajima, N. Orimoto and S. Shoji, *Sens. Actuators, A*, 2005, **119**, 365–371.
23 H. Sato, D. Yagyu, S. Ito and S. Shoji, *Sens. Actuators, A*, 2006, **128**, 183–190.
24 A. D. Stroock and G. J. McGraw, *Philos. Trans. R. Soc. London, Ser. A*, 2004, **362**, 971–986.
25 F. Schonfeld and S. Hardt, *AIChE J.*, 2004, **50**, 771–778.
26 Y. Z. Liu, B. J. Kim and H. J. Sung, *Int. J. Heat Fluid Flow*, 2004, **25**, 986–995.
27 T. G. Kang and T. H. Kwon, *J. Micromech. Microeng.*, 2004, **14**, 891–899.
28 M. Camesasca, I. Manas-Zloczower and M. Kaufman, *J. Micromech. Microeng.*, 2005, **15**, 2038–2044.
29 J. Aubin, D. F. Fletcher, J. Bertrand and C. Xuereb, *Chem. Eng. Technol.*, 2003, **26**, 1262–1270.
30 H. Z. Wang, P. Iovenitti, E. Harvey and S. Masood, *J. Micromech. Microeng.*, 2003, **13**, 801–808.
31 D. G. Hassell and W. B. Zimmerman, *Chem. Eng. Sci.*, 2006, **61**, 2977–2985.
32 C. A. Li and T. N. Chen, *Sens. Actuators, B*, 2005, **106**, 871–877.
33 J. Aubin, D. F. Fletcher and C. Xuereb, *Chem. Eng. Sci.*, 2005, **60**, 2503–2516.
34 J. T. Yang, K. J. Huang and Y. C. Lin, *Lab Chip*, 2005, **5**, 1140–1147.